Mid-IR supercontinuum generation in birefringent, low loss, ultra-high numerical aperture Ge-As-Se-Te chalcogenide step-index fiber

Jayasuriya, D.; Petersen, Christian Rosenberg; Furniss, David; Markos, Christos; Tang, Zhuoqi; Habib, Md Selim; Bang, Ole; Benson, Trevor M.; Seddon, Angela B.

Published in:
Optical Materials Express

Link to article, DOI:
10.1364/OME.9.002617

Publication date:
2019

Document Version
Publisher's PDF, also known as Version of record

Research Article Vol. 9, No. 6 / 1 June 2019 / Optical Materials Express 2617
Optical Materials EXPRESS

Mid-IR supercontinuum generation in birefringent, low loss, ultra-high numerical aperture Ge-As-Se-Te chalcogenide step-index fiber

D. Jayasuriya,[1] C. R. Petersen,[2,3,*] D. Furniss,[1] C. Markos,[2,3] Z. Tang,[1] MD. S. Habib,[4] O. Bang,[2,3] T. M Benson,[1] and A. B Seddon[1]

[1]*Mid-Infrared Photonics Group, George Green Institute for Electromagnetics Research, University of Nottingham, University Park, NG7 2RD Nottingham, United Kingdom*
[2]*DTU Fotonik, Dept. of Photonics Engineering, Technical University of Denmark, Ørsteds Plads 343, 2800 Kongens Lyngby, Denmark*
[3]*NORBLIS IVS, Virumgade 35D, Virum, Denmark*
[4]*CREOL, The College of Optics and Photonics, University of Central Florida, Orlando, FL-32816, USA*
[*]*chru@fotonik.dtu.dk*

Abstract: This work reports on the fabrication and subsequent supercontinuum generation in a Ge-As-Se-Te/Ge-As-Se core/clad chalcogenide step-index fiber with an elliptical-core and an ultra-high numerical aperture of 1.88 ± 0.02 from 2.5 - 15 µm wavelength. The fiber has very low transmission loss of < 2 dB/m from 5-11 µm and a minimum loss of 0.72 ± 0.04 dB/m at 8.56 µm. Supercontinuum spanning from 2.1 µm to 11.5 µm with an average power of ~6.5 mW was achieved by pumping a ~16 cm fiber with a minor/major axis core diameter of 4.2/5.2 µm with 250 fs pulses at 4.65 µm wavelength and a repetition rate of 20.88 MHz. The effect of the elliptical-core was investigated by means of mechanical rotation of the fiber relative to the linear pump polarization, and it was found to cause a shift in the supercontinuum spectral edges by several hundred nanometers.

1. Introduction

In recent years there has been an increasing interest in powerful and versatile broadband light sources for bio-imaging, spectroscopy, microscopy, and sensing applications [1–6]. A principal candidate to fulfil these requirements is optical fiber-based supercontinuum generation (SCG) and specifically mid-infrared (MIR) SCG to cover the molecular fingerprint region (5–15 µm). This region contains most of the strong and distinct fundamental vibrational absorption bands of molecules, which may contribute to a more reliable and accurate molecular analysis. One of the main limitations for achieving fiber-based SCG across the fingerprint region is the need for low-loss optical fibers that are both highly nonlinear and transparent at these wavelengths. Unfortunately, only few types of optical fibers are able to guide light in the fingerprint region, such as polycrystalline silver halides, dielectric coated hollow-cores, chalcohalides, and chalcogenides [7]. While silver halides have been used for beam delivery in e.g. spectroscopic applications they are not suitable for SCG due to the difficulty with producing low-loss, small-core fibers to achieve high nonlinearity [8]. Hollow-core fibers (HCF) have been used primarily for high power laser beam delivery, and while gas-filled HCFs have been demonstrated to produce broadband SCG spanning from UV to MIR this requires ultrashort, megawatt peak power pulses and the extension into the MIR has so far been limited to less than 5 µm [9,10]. On the other hand, chalcohalide and chalcogenide glasses has been shown to produce low-loss and highly nonlinear fibers with a wide MIR transparency, which is why they are considered prime candidates for MIR SCG.

#364566 https://doi.org/10.1364/OME.9.002617
Journal © 2019 Received 8 Apr 2019; revised 8 May 2019; accepted 8 May 2019; published 16 May 2019

Optical Materials EXPRESS

In the past several decades chalcogenide glasses have been reported extensively in the literature [11–15]. They are inorganic materials that are based on one or more of the chalcogen elements S, Se, Te found in the new Periodic Table: Group XVI. The general molecular structure of chalcogenide glasses is expressed as covalent bonds forming an eight electron shell [16]. By melting the covalently bonded solids, comprising chalcogenide elements (S, Se, Te) with Group XV elements (Sb, As) and Group XIV (Ge, Si), glasses with unique optical and semiconducting properties may be obtained [17]. These glasses are suitable for many passive MIR applications such as radiometric thermometry and CO_2 laser power delivery due to their low phonon energy and environmental stability [17–19]. They have also been demonstrated as suitable for broadband MIR SCG due to their high optical nonlinearity [14,20,21]. The broadest MIR SC reported to date spanning from 2-16 µm was achieved using a 14 cm long Ge-Te-AgI chalcohalide core and Ge-Sb-Se chalcogenide cladding step-index fiber (SIF) with a core diameter of 20 µm [22]. Similar results were obtained in a 3 cm long $As_2Se_3/AsSe_2$ SIF with a 15 µm core diameter resulting in SC broadening from 2-15.1 µm [23]. These results were obtained by using a wavelength-tunable MW peak power difference frequency generation (DFG) beamline, which is good for demonstrating the capabilities of the fiber but unsuitable for practical applications. Many other glass systems, such as As-Se/Ge-As-Se [24], Ge-As-Se/Ge-As-S [25], Ge-Sb-Se [26], and Ge-As-Se-Te [27,28] have also been investigated resulting in SC spectra spanning around 1.5 -14 µm.

Among the family of chalcogenides, Te-based glasses have the highest nonlinearity and longest wavelength transmission edge, but Te on its own is not a good glass former. The ternary Ge-As-Te system is known as a poor glass former due to its small glass formation regions [29–31]. Adding Se to the ternary Ge-As-Te system results in a compromise between stable glass forming region and long wavelength transparency [21]. It is reported that a Te content of the Ge-As-Se-Te glass system close to 50 at.% produces the most stable glasses with lowest optical fiber losses. The minimum optical loss for a Ge-As-Se-Te unstructured fiber has been reported to be 0.11 dB/m at 6.6 µm wavelength, with high absorption of H-Se at 4.55 µm and Ge-H at 5 µm wavelength [32]. The minimum optical losses for Ge-As-Se-Te core/cladding fiber have been reported as low as 0.15 dB/m at 6.6 µm wavelength, with intense Se-H impurity bands at 3.5, 4.1 and 4.57 µm wavelength [33].

In this work, we have successfully modelled and fabricated a low-loss $Ge_{16}As_{24}Se_{15.5}Te_{44.5}$ (at.%)/ $Ge_{10}As_{23.4}Se_{66.6}$ (at.%) SIF that has an ultra-high numerical aperture (NA) of ~1.88, which to the best of our knowledge is the highest NA ever reported for a chalcogenide fiber. Fibers of several core diameters were fabricated and tested for SCG by pumping with a kW peak power DFG source delivering 250 fs pulses at 4.65 µm wavelength and with a pulse repetition rate of 20.88 MHz.

2. Fiber fabrication

The core/cladding, Ge-As-Se-Te/Ge-As-Se SIF was fabricated using the melt-quenching technique. Note that only the core glass composition (Ge-As-Se-Te glass) was distilled to obtain lower optical loss. Both core and cladding glasses were prepared using purification by heat treatment. Oxides being more volatile than the elemental precursors, As (7N purity, Furakawa Denshi) and Se (5N purity, Materion) was purified by heat-treating under vacuum (~10^{-3} Pa) at 310 °C and 260 °C respectively. Ge (5N purity, Materion) and Te (5N purity, Materion) were untreated. Subsequently the elements were batched in an MBraun glove-box (≤ 0.1 ppm H_2O and O_2) under nitrogen atmosphere into a vitreous silica ampoule (<1 ppmOH, Multilab ltd, UK); which was etched using 40% $^{v}/_{v}$ hydrofluoric acid (HF), rinsed with deionised water and air/vacuum baked (under vacuum ~10^{-3} Pa) at 1000 °C for 6 h in a vertical furnace (TF105/4.5/IZF, Instron) to drive off physisorbed and chemisorbed water from inside surface of the silica glass ampoule. The silica ampoule containing the batched elements then was sealed under vacuum using an

Optical Materials EXPRESS

oxy propane torch (~10^{-3} Pa) and placed in a rocking furnace for ~ 12 h to melt/homogenise at ~ 750 °C for the core glass and ~ 800 °C for the cladding glass. The core and the cladding glasses were removed from the rocking furnace at 750 °C and 800 °C, respectively, which started the quenching process. Quenching usually took ~ 3 min. Glasses were then transferred to the annealing furnace and annealed ~ 1 h at the glass transition temperature (T_g) and then cooled with the furnace at ~ 10°C/h. The Ge-As-Se cladding glass rod prepared was 29 mm diameter and 45 mm length.

The Ge-As-Se-Te core glass was distilled with 300 ppm of Al (5N purity, Alfa Aesar) as an oxide getter, and 900 ppm of $TeCl_4$ (5N purity, Alfa Aesar) as a hydride getter. In preparation for distillation, a preliminary melt was done in a silica glass ampoule with $TeCl_4$ (5N purity, Alfa Aesar) added to the purified (As and Se) and as supplied precursors (Ge, Te) in a MBraun glove-box (≤ 0.1 ppm H_2O and O_2). As described above this was then melted-quenched and annealed. The as-annealed glass rod from the preliminary melt was then taken out of the silica glass ampoule inside the MBraun glove-box (≤ 0.1 ppm H_2O and O_2) and was batched into a silica distillation rig with the addition of Al as an oxide getter. The in house designed silica distillation rig (Multilab ltd, UK) was HF etched and baked similar to the silica ampoule as mentioned above prior to the batch. After sealing the charge end (A-A) of the distillation rig, using an oxy-propane (BOC) torch, which contains the getters and the as annealed glass (Fig. 1), it was then placed in the distillation set up. Using a two-zone furnace (Fig. 1), zone 1 (charge end) and zone 2 (distil end) was heated up to ~ 500 °C for an hour so the getters react with the glass melt while under open vacuum (~10^{-3} Pa). Then the charge end was heated up to ~ 800 °C and the distillate-end temperature was reduced to ~ 200 °C, so that the low vapour pressure impurities were held in the charge end (e.g. Al_2O_3) and high vapour pressure impurities were taken away with the vacuum (e.g. HCl, CCl_4). Note that when the charge end started to heat up from 500 to 800 °C the distillate-end was sealed off under vacuum (B-B) assuming the residual HCl has been taken away with the applied vacuum. Then the distillation was carried out to completion, condensing the glass in the distillate-end. After cooling down the distillation rig, it was sealed at point C-C and placed in a rocking furnace for ~ 2 h at 750 °C to melt and homogenise, followed by quenching and annealing at T_g (~ 176 ± 2 °C). The Ge-As-Se-Te core glass rod prepared was 10 mm diameter and 90 mm length.

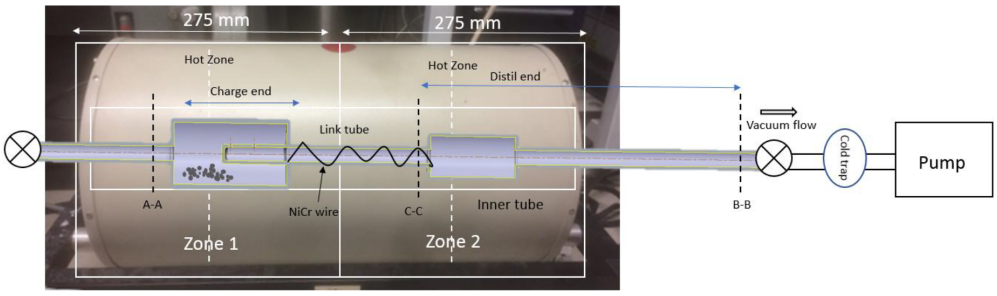

Fig. 1. Distillation set up schematic for partially open or open distillations with flow directions and sealing points indicated: (a) using a two-zone furnace and (b) using a clam shell furnace.

Due to the disparate nature of the viscosities of the core (at 236 °C log viscosity of 7 ± 0.2 Pas) and cladding (at 236 °C log viscosity of 7.5 ± 0.2 Pas) glasses the small core (~ 6 µm diameter) SIF was fabricated using a double rod in tube method [34] (Fig. 2) using a in house built Heathway draw-tower. The Ge-As-Se cladding glass was extruded to a 150 mm long tube at ~ 240°C (Fig. 2(b)) with 2 mm inner diameter (ID) and 10 mm outer diameter (OD), which was cut into two 70 mm length tubes. The Ø 10 mm x 90 mm distilled Ge-As-Se-Te core glass

Optical Materials EXPRESS

was drawn to cane with ~ 1.75 mm diameter that was inserted into the first cladding tube and drawn to intermediate cane ~ 1.75 mm diameter (Fig. 2(c)). The intermediate cane was inserted into the second tube and drawn to optical fiber controlling the OD of the optical fiber to achieve the desired core diameter (Fig. 2(e)). The only considerable disadvantage of the rod in tube method over co-extrusion of a preform is that, with the rod and tube method controlling the core/cladding geometry is much more difficult i.e. core geometry tends to be elliptical. However with disparate core/cladding viscosities this method is more suitable than co-extruding. The final optical fibers fabricated were as follows: core diameter ~ 4 µm with cladding diameter 152 ±7 µm, core diameter ~ 5 µm with cladding diameter ~ 200 µm, core diameter ~ 6 µm with cladding diameter 229 ±5 µm, core diameter ~ 8 µm with cladding diameter ~ 300 µm and core diameter ~ 10 µm with cladding diameter 381 ±5 µm**.**

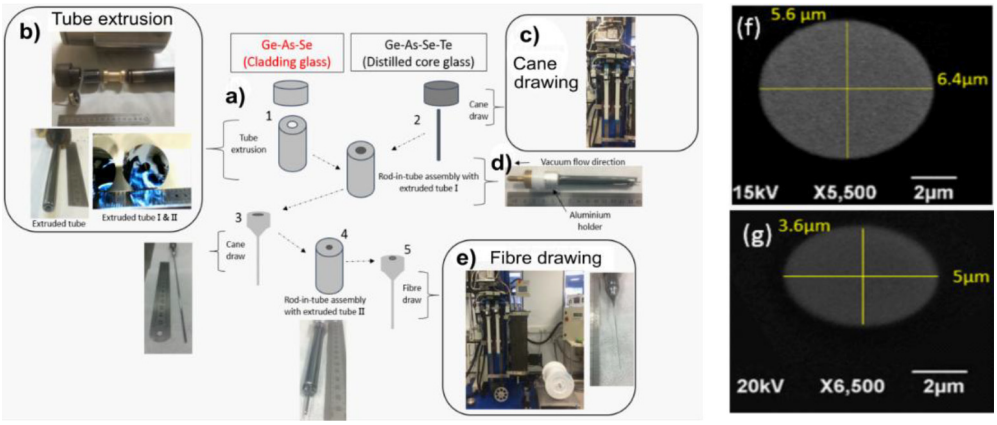

Fig. 2. (a) Schematic diagram of the rod-in-tube method of small core SIF fabrication, (b) extrusion components (c) cane drawing setup (d) aluminium holder for rod-in-tube method (e) fiber drawing set up; (f) SEM cross-section images of fabricated ~ 6 µm core diameter SIF and (g) ~ 4 µm core diameter SIF.

The onset-T_g [35] of the core/cladding glass was measured using differential scanning calorimetry (DSC, DSCQ10 thermal analyzer), sealing approximately 30 mg of chalcogenide glass in a lidded Al crucible and heating/cooling at 10°C/min under argon (BOC, UK) flow, 3 times to obtain a comparable thermal history. Onset-T_g was taken as the mean of the 2nd and 3rd runs [35]. X-ray diffraction (XRD) patterns were used to investigate amorphicity of the annealed products using a Siemens D500 diffractometer with CuKα radiation, 10^0 to 70^0 2θ, step size of 0.05^0 and 40 sec time/step. Small rod samples for viscosity/temperature measurement were sliced from an extruded, unstructured chalcogenide glass preform, of ~ 5 mm in diameter and ~ 3 mm long, with flat and parallel top and bottom surfaces. Viscosity/temperature measurements were carried out on a Perkin Elmer thermomechanical analysis (TMA), set up for parallel-plate viscometry. Measurements reported here, were made between log viscosity 10^4 Pas and 10^8 Pas, with a load of 50 - 400 mN, applied under a He (BOC, UK) atmosphere. A Bruker FTIR IF 66 spectrometer was used to collect absorption spectra of the bulk chalcogenide samples; these were 2.5 - 3.2 mm optical path length disks with, both circular faces ground parallel and polished to 1 µm finish. A DTGS detector was used with a tungsten (W) filament source and CaF_2 broadband beam splitter for NIR measurements, and a DTGS detector, Globar source and KBr beam splitter for MIR measurements. Fiber loss of the unstructured core glass fiber was measured using the cutback method as described in [36] for a ~ 7.5 m length, ~ 250 µm diameter optical fiber on a Bruker FTIR IF 66 spectrometer; with Globar light source, KBr beam splitter and InSb/MCT detectors cooled with liquid nitrogen. Core/cladding refractive indices were

Optical Materials EXPRESS

measured by IR ellipsometer measurements (IR-VASE MARK II, J.A. Woollam Co.). To confirm the glass compositions, energy dispersive X-ray (EDX) of JEOL 6490 was used.

Both $Ge_{16}As_{24}Se_{15.5}Te_{44.5}$ at.% core glass and $Ge_{10}As_{23.4}Se_{66.6}$ at.% cladding glass was numerically modelled so that they were thermally compatible (T_gs matched) and were of a suitable refractive index difference to achieve a ultra-high NA optical fiber. DSC and XRD curves were used to look for any crystallisation features. Using DSC curves for different glass batches with the same nominal compositions, the T_g was determined to be 176 ± 2°C both for core and cladding glasses. The broad halo nature of the XRD curves suggested that there were no obvious crystallisation peaks (< 5% vol.% crystals) for both core and cladding glasses after fiber drawing at ~ 300°C. For both and cladding synthesised glasses, EDX composition analysis indicated that glasses were within ± 0.5 at.% of the nominal composition. Considering the accuracy of the equipment (JEOL 6490LV SEM) to be ± 0.5 at.%, an elemental composition standard deviation of ± 0.5 at.% is deemed acceptable.

3. Optical characterization

For SCG, it is critical that the glasses are high purity to attain low loss optical fiber. Especially considering high losses in Se-Te based glasses due to metallic characteristics with the addition of Te. Figure 3(a) shows the comparison of MIR transmission spectra of the core glass Ge-As-Se-Te, partially-purified and distilled with oxide and hydride getters. It should be noted that addition of getters to the batch, could increase the background losses of the final fiber. Hence it should be a balance between prior purification of elements before distilling and application use, since more getters present in the glass would contribute towards increasing the scattering losses [34,37]. Introducing $TeCl_4$ into the glass has a high possibility of introducing inclusions in the final fiber and this was observed in one of the preliminary optical fibers that was assumed as residual HCl. The oxide getter and the hydride getter were efficient as scavenging agents reducing Se-H, OH, H_2O, Ge-O impurity bands.

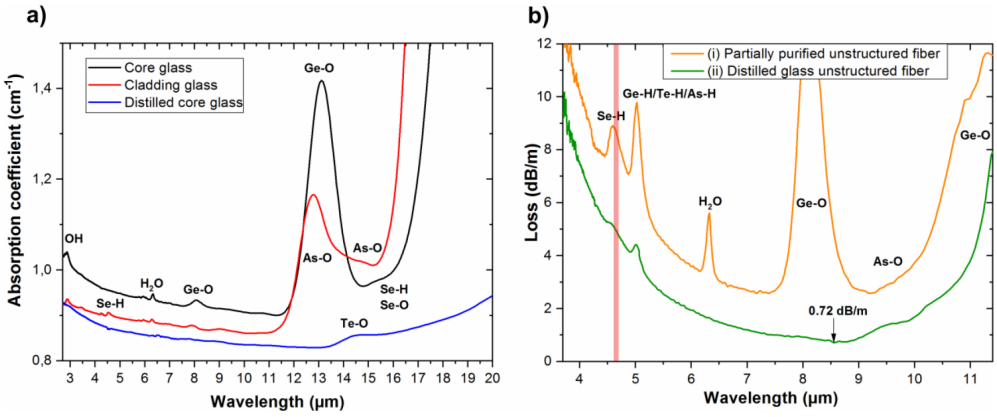

Fig. 3. (a) FTIR measurement of 2.5 mm optical path length samples of: partially purified core glass (black), partially purified cladding glass (red), and distilled core glass (blue). Main impurity bands are indicated. (b) Unstructured fiber loss of partially purified (orange) of fiber length 2.081 m, and distilled core glass with 350 ppmw Al oxide getter and 900 ppmw $TeCl_4$ hydride getter (green) of fiber length 4.580 m. The red shaded area illustrates the pump wavelength. Refer to Table 1 for extinction coefficients and impurity concentrations.

It is also observed that for the Ge-As-Se-Te glass system, the background loss drops down significantly after 5 μm wavelength (Fig. 3(a)), which is indicative of the glass system being more transparent at the long wavelengths. In order to avoid excess scattering losses, it is

Optical Materials EXPRESS

recommended to use hydride getter doping level of 900 - 1000 ppm and oxide getter doping levels of 200 - 300 ppm, depending on the prior purification of elements. Due to the small core in the core/cladding optical fibers fabricated, accurate loss measurements could not be obtained using the FTIR system. Figure 3(b) presents the optical fiber loss spectra of the unrestructured core glass composition, $Ge_{16}As_{24}Se_{15.5}Te_{44.5}$ (at.%) with different preparation methods; (i) partially-purified, (ii) distilled with Al (0.03 wt.%) and $TeCl_4$ (0.09 wt.%). Lowest loss achieved was 0.72 ± 0.04 dB/m at 8.56 µm and < 2 dB/m from 5-11 µm onwards with the distilled glass. Comparing the impurity bands relative to the background, four major absorption bands (H-Se [38], Ge-H [39], H_2O, and Ge-O) and several minor bands (Si-O/As_4O_6) were observed for the Ge-As-Se-Te system. Main impurity bands at 2.75 µm and 2.85 µm due to O-H, 4.6 µm due to Se-H, 5 µm due to Ge-H/Te-H/As-O, 6.29 µm due to molecular H_2O, 8.05 µm and 13.01 due to Ge-O, and at 9.5 µm due to ≡[Si-O]- and As_4O_6 [26–31] could be observed in the partially purified (i.e. only As and Se elemental precursors were pre-purified by heat treatment) core and cladding glasses and reduced/removed in the distilled core glass (in blue).

Table 1 lists absorption bands, estimated concentration of impurity absorptions and loss contribution for this glass system. Using known extinction coefficients, concentration of impurities was determined for the Ge-As-Se-Te glass system. Concentration of H-Se impurity was determined using 1.103 dB/m/ppm that Churbanov *et. al.* [40] obtained for As_2Se_3 glass. Due to similar glass properties of Ge-As-Se-Te glass matrix the variation of the extinction coefficient is assumed small. The extinction coefficient of the Ge-O combination band at 8.1 µm was determined as 2.61 dB/m/ppm for oxide doped telluride glasses by Nishii *et al.* [41]. No literature could be found on the extinction coefficient of the H_2O band at 6.3 µm for telluride glasses. However Ernsberger [42] has reported an extinction coefficient of 16 liters $mol^{-1}cm^{-1}$ (33.969 dB/m/ppm) around 6 µm for liquid water in a silicate glass. It should be pointed out that on gettering the Ge-As-Se-Te glass system with Al + $TeCl_4$, absorption band intensities of H-Se, Ge-H, H_2O and Ge-O were reduced by a factor of more than 5, or completely eliminated, compared to fiber fabricated with partially purified elements.

As mentioned earlier the lowest loss for a Ge-As-Se-Te glass system ($Ge_{30}As_{10}Se_{30}Te_{30}$ (at.%)) was reported by Sanghera *et al.* [32] as 0.11 dB/m at 6.6 µm. To obtain the lowest loss Sanghera *et al.* [32] used only 10 ppmw of Al as an oxide getter. However, comparing the estimated concentration impurity levels of H-Se, oxide and water of the lowest loss $Ge_{30}As_{10}Se_{30}Te_{30}$ (at.%) optical fiber spectrum with the lowest loss $Ge_{16}As_{24}Se_{15.5}Te_{44.5}$ (at.%) optical fiber spectrum reported here ((ii) in Fig. 3(b)), it could be observed that: for $Ge_{16}As_{24}Se_{15.5}Te_{44.5}$(at.%) 0.16 ppm-wt of H-Se is reported here with completely eliminated oxide and water impurities, while in the $Ge_{30}As_{10}Se_{30}Te_{30}$ (at.%) optical fiber spectrum H-Se, oxide and water were reported as 3.23 ppm-wt, 0.06ppm-wt and <0.01 ppm-wt, respectively. Although a direct comparison of the loss spectra is not possible due to the compositional differences, it could be concluded that distillation

Table 1. Absorption bands, estimated concentration of impurity absorptions and loss contribution for the $Ge_{16}As_{24}Se_{15.5}Te_{44.5}$ (at.%) glass system (see Fig. 3(b)). (i) precursors partially purified (i.e. only As and Se elemental precursors were purified by heat treatment); (ii) partially open vacuum distillation with 350 ppmw Al oxide getter and 900 ppmw $TeCl_4$ hydride getter.

Wavelength / (µm)	Absorption band	Loss contribution/ (dB/m)		Estimated concentration/ (ppm-wt)	
		(i)	**(ii)**	**(i)**	**(ii)**
4.6	H-Se [38] [40]	1.8	0.18	1.63	0.16
5.0	Ge-H [39]	3.9	0.68	-	-
6.3	H-O-H [42]	2.3	-	0.07	-
8.1	Ge-O [41]	24	-	9.20	-
9.5	Si-O/As_4O_6	-	0.09	-	-

Optical Materials EXPRESS

getting would depend on the end objective i.e. trying to achieve the lowest loss possible or trying to reduce/remove impurity bands for applicational purposes.

The refractive indices of the core/cladding glasses and calculated NA is shown in Fig. 4(a). These were measured using IR ellipsometry (measurements were carried out by J.A. Woollam Co. using IR-VASE MARK II) and fitted to a two-term Sellmeier model. The Sellmeier fit for the core glass presented a R-squared value of 1, and a SSE (sum of squared error) of 3.9×10^{-5}, and for the cladding glass a R-squared value of 0.9999, and a SSE of 3.7×10^{-4}, indicative of excellent fits. The core and cladding refractive indices between wavelengths 2.5 - 15 µm covering the finger print region (accepted as 6 -15 µm) were measured as 3.22 - 3.16 (core glass) and 2.60 - 2.56 (cladding glass) respectively, giving a calculated ultra-high NA of 1.88 ± 0.02 for the SIF over the 2.5 - 15 µm wavelength range. A high numerical aperture is important because it provides tight confinement to the core and thereby increases the effective nonlinearity of the fiber. Furthermore, it provides the means for shifting the zero-dispersion wavelength (ZDW) towards shorter wavelengths by scaling down the core diameter, which would otherwise result in all-normal dispersion [28,43]. Based on our numerical simulations and by extracting the Sellmeier coefficients from the refractive index measurements, the material dispersion for the core and the cladding glass materials were calculated and is presented in Fig. 4(b). The ZDW for the Ge-As-Se-Te glass is at 9.79 µm and the Ge-As-Se is at 6.98 µm, but the ZDW of the Ge-As-Se-Te/Ge-As-Se SIF can be shifted to shorter wavelengths by reducing the core diameter. To illustrate this, the dispersion of the fundamental mode for different circular core diameters was modelled using COMSOL 5.2, and the results are shown in Fig. 5(a). Taking into account that the pump had a maximum tuning wavelength of 4.7 µm, the 4 µm (ZDW at 4.36 µm) and 6 µm (ZDW at 4.9 µm) diameter core SIFs were the best candidates for achieving the broadest possible SC spectrum.

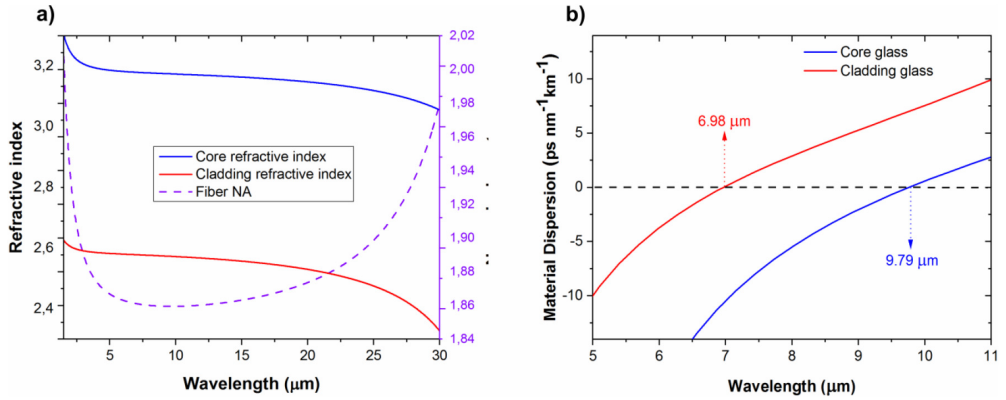

Fig. 4. (a) Refractive index dispersion measurement from 1.5 to 30 µm wavelength for the core glass (blue) and cladding glass (red), and the corresponding numerical aperture of the optical fiber (purple dashed). (b) Material dispersion of the core (black) and cladding (red) glasses indicating a material ZDW at 6.98 µm and 9.79 µm, respectively.

Considering the elliptical shape of the 4 µm core fiber (3.6/5 µm), the fiber was also expected to be highly birefringent, and in fact numerical modelling suggested that the birefringence was as high as 2×10^{-2} at 11.5 µm, as seen in Fig. 5(b), which to the authors' knowledge is higher than any previously reported polarization maintaining chalcogenide fiber. Figure 5(b) shows the dispersion of the slow and fast axes of the fiber, which is seen to cause a shift in the ZDWs of up to several hundreds of nanometers. The 2nd ZDW of the elliptical 4 µm core fiber is estimated to be around 8.5 µm and 8.9 µm for the slow and fast axis, respectively.

Optical Materials EXPRESS

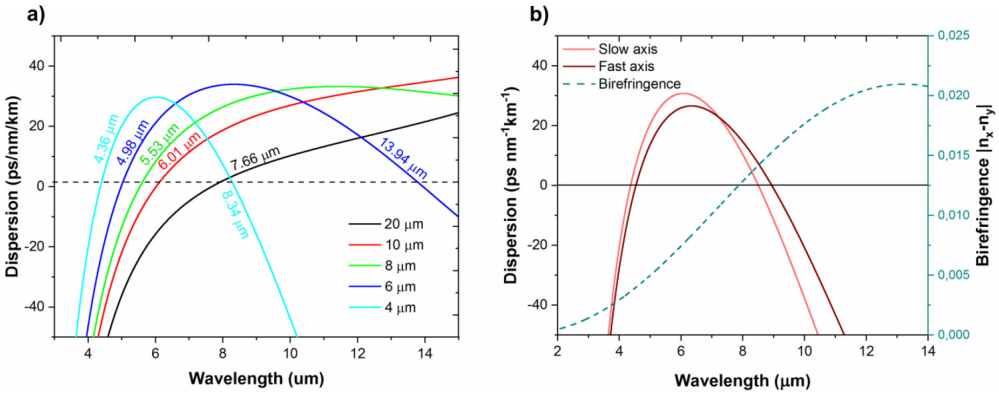

Fig. 5. (a) Calculated dispersion and ZDWs for the fundamental mode of SIFs with varying core diameter (for a circular core structure), modelled using COMSOL 5.2. (b) Calculated birefringence (dashed) and slow/fast axis dispersion (solids) of the 4 µm core diameter elliptical fiber based on actual imported SEM image in Fig. 2(g).

4. Supercontinuum generation

The pump source used in the SCG experiments has been previously reported in [44]. The source produces linearly polarized approximately 250-300 fs pulses at 20.88 MHz repetition rate and is wavelength tunable between 3.7 to 4.7 µm. The MIR beam was coupled to the fiber using a 6 mm focal length (NA = 0.56) black diamond lens with anti-reflection (AR) coating for the 3-5 µm range, and the coupling power was adjusted using a wire grid polarizer. The fiber was mounted on a translation stage using a high precision fiber rotator in order to optimize both the axial position and rotation with respect to the pump polarization. At the output of the fiber the generated continuum was collimated using a 1.87 mm focal length (NA = 0.86) black diamond lens also AR coated for the 3-5 µm range. The collimated beam was subsequently focused using a 100 mm off-axis parabolic mirror onto the input slit of an imaging spectrometer equipped with a 48-element mercury-cadmium-telluride (MCT) detector array to measure the SC spectra. The pump power and output power was measured using a thermal power meter.

Several fibers with different core diameters, but similar lengths were tested. Figure 6(a) show SC spectra for three fibers with a core diameter of 10 µm (11.8 × 8.5 µm), 6 µm (7.6 × 5.5 µm), and 4 µm (5.2 × 4.2 µm), using a length of 18 cm, 16 cm, and 15.5 cm, respectively. For these experiments the wavelength was fixed at 4.65 µm to reduce the absorption, and to pump closer to the ZDW of the fibers for maximum efficiency. The 10 µm fiber had a ZDW of around 6 µm, which means that it was pumped deep in the normal dispersion regime resulting in most of the power remaining near the pump wavelength and exhibiting mainly weak broadening due to self-phase modulation (SPM). The plateau from 6-8 µm is from the long-wavelength edge of the SPM-broadened spectrum crossing the ZDW, thus enabling the generation and possibly fission of solitons that could continue to broaden through collisions. The output power in this case was 18 mW, which corresponds to an estimated launched peak power of 4.1 kW. The 6 µm fiber was pumped very close to the ZDW, which resulted in a much larger part of the pump entering the anomalous dispersion regime causing increased broadening due to soliton dynamics reaching around 9 µm in wavelength. On the short-wavelength side of the spectrum several intense peaks are seen, which is indicative of dispersive wave generation.

The broadest spectrum spanning from 1.5 to 11.6 µm was achieved from the 4 µm core diameter SIF. The maximum average pump power before the coupling lens was ~36 mW, and the output power after the collimating lens was measured to be ~ 6.5 mW which corresponds to ~34% transmission taking into account the Fresnel reflections at the air-glass interfaces. From this the

Optical Materials EXPRESS

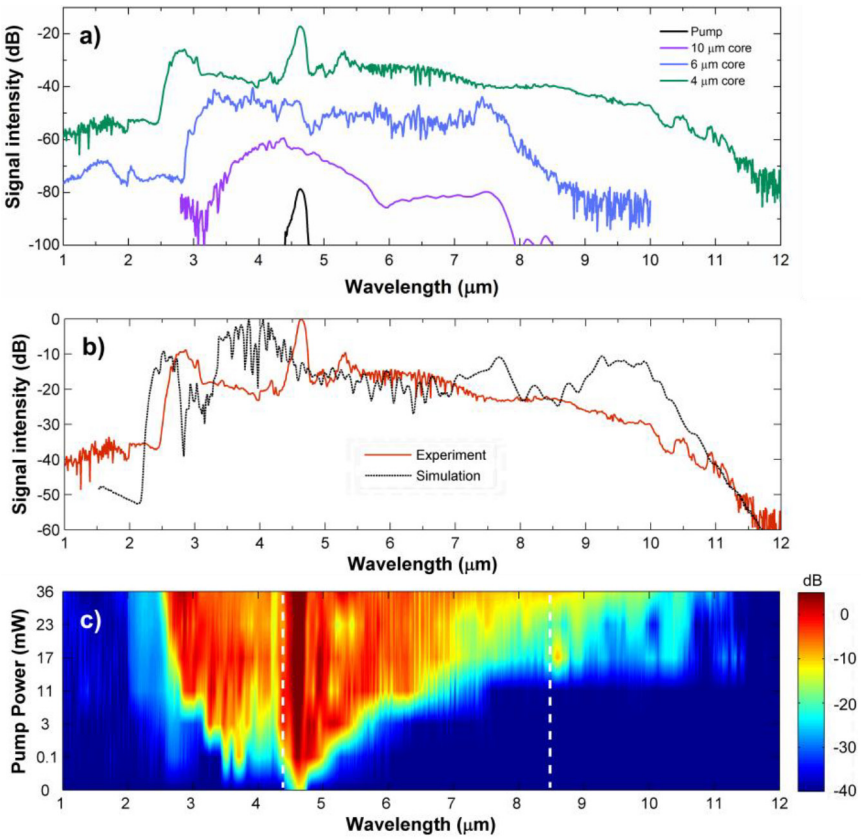

Fig. 6. (a) SC spectra obtained from fibers with around 4 μm, 6 μm, and 10 μm core diameters of lengths 155 mm, 161 mm, and 180 mm, respectively. (b) Comparison between experiment and simulation output spectra for the 4 μm core fiber assuming 1.5 kW coupled peak power. (c) Measured spectral evolution with increasing pump power coupled to the 4 μm core diameter fiber. The dashed lines show the position of the ZDWs of the slow axis polarization.

coupled peak power is estimated to be around 1.5 kW. For the 4 μm core fiber the first ZDW was located at 4.36 μm, which meant most of the power should have initially gone towards the longer wavelengths. However, for this measurement, a significant residual pump peak was observed. By numerical integration the residual pump is estimated to account for about 3.24 mW, so the coupling efficiency to the core could be as low as 17%. This was likely due to the smaller core diameter, which resulted in part of the pump being guided in the cladding and thus not contributing towards spectral broadening. Nevertheless, the fiber produced the broadest continuum in all experiments, which is likely due to a combination of the very high nonlinearity of the smaller core together with the introduction of a second ZDW around 8.5 μm (slow axis), which resulted in the emission of red-shifted dispersive waves (RDWs). These RDWs is seen in Fig. 6(c) initially as a peak at 8.6 μm with a broad tail extending to 11.5 μm emerging once the pump power was sufficient for the broadening to reach the second ZDW. With increasing pump power the spectral edge remained at 11.5 μm, but the overall flatness of the spectrum improved. Increasing the pump power beyond approximately 36 mW led to damage of the fiber end facet, which was found to be consistent between measurements. The damage threshold was likely affected by the rapidly increasing absorption below the pump wavelength, and possibly

Optical Materials EXPRESS

mechanical stress at the core/cladding interface. Nanoimprinted anti-reflective end-caps with a similar core material composition to reduce both the Fresnel reflections and the intensity on the fiber launch end, or a thin film coating of damage resistant material (such as Al_2O_3) would allow for more power to be coupled to the fiber [45,46]. Evaluating the reported literature [25,44 47] of SIF SC spectra generated in the MIR region with MHz repetition rate pumping schemes, the SC generated here in the 4 μm core diameter SIF is among the broadest reported to date.

To further investigate the SCG dynamics, numerical pulse propagation simulations were carried out using the same implementation as in Ref. [9] with 2^{16} number of points and a temporal resolution of 556 fs. The Raman response coefficients were assumed to be $f_R = 0.115, \tau_1 = 23.1$ fs, $\tau_2 = 195$ fs. From COMSOL the nonlinear coefficient (γ) was calculated to be 5.36 $m^{-1}W^{-1}$ at the pump wavelength, and due to the high NA the core confinement was >90% from 1-7.5 μm, >80% until 10 μm, and >70% until 11.5 μm. Figure 6(b) show a comparison between the experimental and simulated output spectra assuming 250 fs pulse duration and 1.5 kW of coupled peak power. The comparison shows that the simulation is able to reproduce some of the qualitative features of the spectrum, namely the distinct DW peak at the short-wavelength edge and RDWs at the long-wavelength edge (peak from 9-10.5 μm). However, while the long-wavelength edge matches fairly well, the short-wavelength is overestimated by 250 nm, which could be due to a discrepancy in the calculated dispersion and coupled peak power.

The spectral evolution in Fig. 6(c) suggests that the fiber was pumped mainly along the slow axis of the fiber. So to investigate the effect of the pump polarization, the output spectrum was recorded for various degrees of fiber rotation. Because the rotation mount had a ± 5 μm eccentricity, these experiments were performed at lower pump power to avoid fiber damage during rotation and subsequent re-alignment. Alignment of the fiber after each 10° rotation was optimized to obtain the longest wavelength edge. The result is shown in Fig. 7, which shows that the long-wavelength-edge is shifted by more than half a micron during the 90° rotation of the fiber. The corresponding shift in the short-wavelength edge is less clear, but this is also expected from the strong dispersion and high loss at shorter wavelengths. A potential application of this behavior could be for bandwidth selective SCG, where tuning of the 2nd ZDW through fiber (polarization) rotation could enable switching between a continuum with reduced bandwidth but higher power spectral density (PSD), or increased bandwidth and lower PSD.

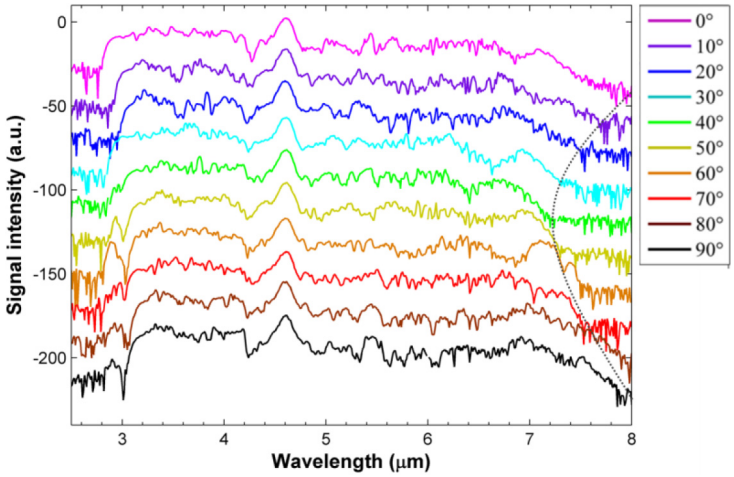

Fig. 7. Measured output spectra as a function of fiber rotation at reduced pump power of ~20 mW to avoid damage from beam offset. The dashed line show the trend in the long-wavelength edge of the spectra.

Optical Materials EXPRESS

In conclusion, ultra-high-NA small-core SIFs with core and cladding made from $Ge_{16}As_{24}Se_{15.5}Te_{44.5}$ (at.%) and $Ge_{10}As_{23.4}Se_{66.6}$ (at.%), respectively, were successfully fabricated and subsequently tested for MIR supercontinuum spectrum generation. The core glass composition was distilled to achieve a low loss optical spectrum reducing or removing any oxide and hydride impurities. A minimum fiber optical loss for the distilled nominal core glass composition ($Ge_{16}As_{24}Se_{15.5}Te_{44.5}$ (at.%)) of 0.72 dB/m at 8.56 μm was achieved. Future distillation of the cladding glass will further lower the fiber loss at the longer wavelengths where the fundamental mode has a significant overlap with the cladding (~31% cladding overlap at 12 μm wavelength for the 4 μm core fiber), which could lead to further spectral extension. Note that the Ge-As-Se-Te/Ge-As-Se, core/cladding optical fiber has the highest calculated numerical aperture reported up to date (>1.86). Following the fabrication of the high-NA small core SIF, a DFG source was used to pump the optical fiber at 4.65 μm wavelength with a pulse duration of 250 fs at a repetition rate of 20.88 MHz. The broadest MIR SC achieved was 1.5 - 11.6 μm with total output power of 6.5 mW, corresponding to an estimated launched peak power of 1.5 kW. Such a broadband, spatially coherent, MHz MIR light source could be applied to a number of applications, including environmental multispecies gas spectroscopy and micro-spectroscopy of tissues for cancer diagnosis.

Funding

Innovationsfonden (4107-00011A); Det Frie Forskningsråd (DFF) (4184-00359B); European Cooperation in Science and Technology (COST); University of Nottingham.

Acknowledgements

D. Jayasuriya acknowledges his PhD Scholarship award and travel award from the University of Nottingham, UK. T. M. Benson and A. B. Seddon acknowledge funding from EU COST MP1401 "Advanced fibre laser and coherent source as tools for society, manufacturing and lifescience".

References

1. C. R. Petersen, N. Prtljaga, M. Farries, J. Ward, B. Napier, G. R. Lloyd, J. Nallala, N. Stone, and O. Bang, "Mid-infrared multispectral tissue imaging using a chalcogenide fiber supercontinuum source," Opt. Lett. **43**(5), 999–1002 (2018).
2. Y.-P. Tseng, P. Bouzy, C. Pedersen, N. Stone, and P. Tidemand-Lichtenberg, "Upconversion raster scanning microscope for long-wavelength infrared imaging of breast cancer microcalcifications," Biomed. Opt. Express **9**(10), 4979–4987 (2018).
3. N. M. Israelsen, C. R. Petersen, A. Barh, D. Jain, M. Jensen, G. Hannesschläger, P. Tidemand-Lichtenberg, C. Pedersen, A. Podoleanu, and O. Bang, "Real-time high-resolution mid-infrared optical coherence tomography," Light: Sci. Appl. **8**(1), 11 (2019).
4. A. B. Seddon, B. Napier, I. Lindsay, S. Lamrini, P. M. Moselund, N. Stone, O. Bang, and M. Farries, "Prospective on using fibre mid-infrared supercontinuum laser sources for in vivo spectral discrimination of disease," Analyst **143**(24), 5874–5887 (2018).
5. C. R. Petersen, P. M. Moselund, L. Huot, L. Hooper, and O. Bang, "Towards a table-top synchrotron based on supercontinuum generation," Infrared Phys. Technol. **91**, 182–186 (2018).
6. M. K. Dasa, C. Markos, M. Maria, C. R. Petersen, P. M. Moselund, and O. Bang, "High-pulse energy supercontinuum laser for high-resolution spectroscopic photoacoustic imaging of lipids in the 1650-1850 nm region," Biomed. Opt. Express **9**(4), 1762 (2018).
7. J. Haas and B. Mizaikoff, "Advances in Mid-Infrared Spectroscopy for Chemical Analysis," Annu. Rev. Anal. Chem. **9**(1), 45–68 (2016).
8. G. Tao, H. Ebendorff-Heidepriem, A. M. Stolyarov, S. Danto, J. V. Badding, Y. Fink, J. Ballato, and A. F. Abouraddy, "Infrared fibers," Adv. Opt. Photonics **7**(2), 379–458 (2015).
9. A. I. Adamu, M. S. Habib, C. R. Petersen, J. E. A. Lopez, B. Zhou, A. Schülzgen, M. Bache, R. Amezcua-Correa, O. Bang, and C. Markos, "Deep-UV to Mid-IR Supercontinuum Generation driven by Mid-IR Ultrashort Pulses in a Gas-filled Hollow-core Fiber," Sci. Rep. **9**(1), 4446 (2019).
10. C. Markos, J. C. Travers, A. Abdolvand, B. J. Eggleton, and O. Bang, "Hybrid photonic-crystal fiber," Rev. Mod. Phys. **89**(4), 045003 (2017).
11. K. J. Rao, *Chalcogenide Glasses in Structural Chemistry of Glasses* (Elsevier, 2002), Chapter 13, 513–534.

Optical Materials EXPRESS

12. D. Lezal, J. Pedlikova, and J. Zavadil, "Chalcogenide glasses for optical and photonics application," Optoelectron.: Adv. Mater. Devices **6**(1), 133–137 (2004).
13. A. B. Seddon, "Chalcogenide glasses: a review of their preparation, properties and applications," J. Non-Cryst. Solids **184**, 44–50 (1995).
14. A. Zakery and S. R. Elliott, "Optical properties and applications of chalcogenide glasses: a review," J. Non-Cryst. Solids **330**(1-3), 1–12 (2003).
15. J. A. Savage and S. Nielsen, "Chalcogenide Glasses Transmitting in the Infrared Between 1 and 20 μm - A State of the Art Review," Infrared Phys. **5**(4), 195–204 (1965).
16. E. Mammadov, D. Bobela, A. Reyes, S. Mehdiyeva, and P. C. Taylor, "Magnetic resonance study of arsenic bonding sites in ternary chalcogenide glasses," Solid State Commun. **151**(20), 1459–1462 (2011).
17. S. Sanghera, L. B. Shaw, and D. Aggarwal, "Applications of chalcogenide glass optical fibres," C. R. Chim. **5**(12), 873–883 (2002).
18. J. Nishii, S. Morimoto, I. Inagawa, R. Lizuka, and T. Yamashita, "Recent advances and trends in chalcogenide glass fiber technology: a review," J. Non-Cryst. Solids **140**, 199–208 (1992).
19. M. Maeda and N. Y.- Zoe, *Chemical Sensor Technology* 3rd ed. (Elsevier, 1991), p. 185.
20. I. Inagawa, R. Iizuka, T. Yamagishi, and R. Yokota, "Optical and Thermal Properties of Chalcogenide Ge-As-Se-Te Glasses for IR Fibers," J. Non-Cryst. Solids **95-96**, 801–808 (1987).
21. V. K. Tikhomirov, D. Furniss, A. B. Seddon, J. A. Savage, P. D. Mason, D. A. Orchard, and K. L. Lewis, "Glass formation in the Te-enriched part of the quaternary Ge-As-Se-Te system and its implication for mid-infrared optical fibres," Infrared Phys. Technol. **45**(2), 115–123 (2004).
22. Z. Zhao, B. Wu, X. Wang, Z. Pan, Z. Liu, P. Zhang, X. Shen, Q. Nie, S. Dai, and R. Wang, "Mid-infrared supercontinuum covering 2.0-16 μm in a low-loss telluride single-mode fiber: Mid-infrared supercontinuum covering 2 μm in a low-loss telluride single-mode fiber," Laser Photonics Rev. **11**(2), 1700005 (2017).
23. T. Cheng, K. Nagasaka, T. H. Tuan, X. Xue, M. Matsumoto, H. Tezuka, T. Suzuki, and Y. Ohishi, "Mid-infrared supercontinuum generation spanning 2.0 to 15.1 μm in a chalcogenide step-index fiber," Opt. Lett. **41**(9), 2117–2120 (2016).
24. C. R. Petersen, U. Møller, I. Kubat, B. Zhou, S. Dupont, J. Ramsay, T. Benson, S. Sujecki, N. Abdel-Moneim, Z. Tang, D. Furniss, A. Seddon, and O. Bang, "Mid-infrared supercontinuum covering the 1.4–13.3 μm molecular fingerprint region using ultra-high NA chalcogenide step-index fibre," Nat. Photonics **8**(11), 830–834 (2014).
25. B. Zhang, Y. Yu, C. Zhai, S. Qi, Y. Wang, A. Yang, X. Gai, R. Wang, Z. Yang, and B. Luther-Davies, "High Brightness 2.2-12 μm Mid-Infrared Supercontinuum Generation in a Nontoxic Chalcogenide Step-Index Fiber," J. Am. Ceram. Soc. **99**(8), 2565–2568 (2016).
26. H. Ou, S. Dai, P. Zhang, Z. Liu, X. Wang, F. Chen, H. Xu, B. Luo, Y. Huang, and R. Wang, "Ultrabroad supercontinuum generated from a highly nonlinear Ge–Sb–Se fiber," Opt. Lett. **41**(14), 3201–3204 (2016).
27. Z. Zhao, X. Wang, S. Dai, Z. Pan, S. Liu, L. Sun, P. Zhang, Z. Liu, Q. Nie, X. Shen, and R. Wang, "1.5–14 μm mid-infrared supercontinuum generation in a low-loss Te-based chalcogenide step-index fiber," Opt. Lett. **41**(22), 5222–5225 (2016).
28. N. Zhang, X. Peng, Y. Wang, S. Dai, Y. Yuan, J. Su, G. Li, P. Zhang, P. Yang, and X. Wang, "Ultrabroadband and coherent mid-infrared supercontinuum generation in Te-based chalcogenide tapered fiber with all-normal dispersion," Opt. Express **27**(7), 10311–10319 (2019).
29. A. R. Hilton, C. E. Jones, and M. Bran, "Non-oxide IVA — VA — VIA chalcogenide glasses .* Part i . Glass-forming regions and variations in physical properties," Physics and Chemistry of Glass volume 7 (1966).
30. J. A. Savage, *Infra-Red Optical Materials and Their Antireflecion Coatings*" W. T. Welfored, ed. (Adam Hilger Ltd, n.d.).
31. Z. U. Borisova, *Glassy Semiconductors* (Plenum, 1981).
32. J. S. Sanghera, V. Q. Nguyen, P. C. Pureza, F. H. Kung, R. Miklos, and I. D. Aggarwal, "Fabrication of low-loss IR-transmitting Ge30As10 Se30Te30 glass fibers," J. Lightwave Technol. **12**(5), 737–741 (1994).
33. V. S. Shiryaev, M. F. Churbanov, E. M. Dianov, V. G. Plotnichenko, J. L. Adam, and J. Lucas, "Recent progress in preparation of chalcogenide As-Se-Te glasses with low impurity content," J. Optoelectron. Adv. Mater. **7**(4), 1773–1779 (2005).
34. B. Zhang, W. Guo, Y. Yu, C. Zhai, S. Qi, A. Yang, L. Li, Z. Yang, R. Wang, D. Tang, G. Tao, and B. Luther-Davies, "Low loss, high NA chalcogenide glass fibers for broadband mid-infrared supercontinuum generation," J. Am. Ceram. Soc. **98**(5), 1389–1392 (2015).
35. D. Furniss and A. B. Seddon, "Thermal Analysis of Inorganic Compound Glasses and Glass-Ceramics, in Principles and Applications of Thermal Analysis" P. Gabbott, ed. Blackwell Publ. Ltd Oxf. UK (2008).
36. Z. Tang, V. S. Shiryaev, D. Furniss, L. Sojka, T. M. Benson, A. B. Seddon, and M. F. Churbanov, "Low loss Ge-As-Se chalcogenide glass fiber, fabricated using extruded preform, for mid- infrared photonics," Opt. Mater. Express **5**(8), 1722–1737 (2015).
37. M. F. Churbanov, V. S. Shiryaev, A. I. Suchkov, A. A. Pushkin, V. V. Gerasimenko, R. M. Shaposhnikov, E. M. Dianov, V. G. Plotnichenko, V. V. Koltashev, Y. N. Pyrkov, J. Lucas, and J.-L. Adam, "High-purity As-S-Se and As-Se-Te glasses and optical fibers," Inorg. Mater. **43**(4), 441–447 (2007).
38. C. T. Moynihan, P. B. Macedo, M. S. Maklad, R. K. Mohr, and R. E. Howard, "Intrinsic and Impurity Infrared-Absorption in As_2Se_3 Glass," J. Non-Cryst. Solids **17**(3), 369–385 (1975).

Optical Materials EXPRESS

39. G. G. Devyatykh, M. F. Churbanov, I. V. Scripachev, and E. M. Dianov, "Middle infrared As-S, As-Se, Ge-As-Se chalcogenide glass fibres," Int. J. Optoelectron. **7**, 237–254 (1992).
40. M. F. Churbanov, I. V. Scripachev, and V. G. Borisevich, "Effect of Hydrogen Impurity on Optical Properties of As–Se and As–S Glass Systems," *Cent. Natl. Telecommun. Lannion Fr. 152–55 in Extended Abstracts of the 8th International Symposium on Halide Glasses Perros-Guirec*, France, September 22–24 (1992).
41. J. Nishii, T. Yamashita, and T. Yamagishi, "Oxide impurity absorptions in Ge-Se-Te glass fibres," J. Mater. Sci. **24**(12), 4293–4297 (1989).
42. F. M. Ernsberger, "Molecular Water in Glass," J. Am. Ceram. Soc. **60**(1-2), 91–92 (1977).
43. I. Kubat, C. S. Agger, U. Møller, A. B. Seddon, Z. Tang, S. Sujecki, T. M. Benson, D. Furniss, S. Lamrini, and K. Scholle, *et al.*, "Mid-infrared supercontinuum generation to 12.5 μm in large NA chalcogenide step-index fibres pumped at 4.5 μm," Opt. Express **22**(16), 19169–19182 (2014).
44. C. R. Petersen, R. D. Engelsholm, C. Markos, L. Brilland, C. Caillaud, J. Trolès, and O. Bang, "Increased mid-infrared supercontinuum bandwidth and average power by tapering large-mode-area chalcogenide photonic crystal fibers," Opt. Express **25**(13), 15336–15347 (2017).
45. A. Sincore, J. Cook, F. Tan, A. El Halawany, A. Riggins, S. McDaniel, G. Cook, D. V. Martyshkin, V. V. Fedorov, S. B. Mirov, L. Shah, A. F. Abouraddy, M. C. Richardson, and K. L. Schepler, "High power single-mode delivery of mid-infrared sources through chalcogenide fiber," Opt. Express **26**(6), 7313–7323 (2018).
46. M. R. Lotz, C. R. Petersen, C. Markos, O. Bang, M. H. Jakobsen, and R. Taboryski, "Direct nanoimprinting of moth-eye structures in chalcogenide glass for broadband antireflection in the mid-infrared," Optica **5**(5), 557–563 (2018).
47. D. D. Hudson, S. Antipov, L. Li, I. Alamgir, T. Hu, M. E. Amraoui, Y. Messaddeq, M. Rochette, S. D. Jackson, and A. Fuerbach, "Toward all-fiber supercontinuum spanning the mid-infrared," Optica **4**(10), 1163–1166 (2017).